Chapter 3

Effect of timing non-idealities on an analog multicarrier system

3.1. Introduction

As discussed in Chapter 1, many publications dealing with data-communication over short length copper wires, e.g. [Farjad-Rad], refer to Pulse Amplitude Modulation (PAM). This modulation method is well suited to a channel with a monotonously decreasing magnitude of the transfer function. However, in some circumstances, for example communication over low-quality PCBs with many impedance discontinuities such as vias, some spectral nulls can be present in the magnitude transfer function. In such cases a linear zero-forcing equalizer in the PAM systems would amplify the noise in the spectral null areas by a large factor [Bingham]. Then orthogonal frequency division multiplexing (OFDM) can be a convenient modulation method, because the signal power distribution can be better tailored to the spectrum. This is also advantageous for channels that suffer from narrowband ingress noise. In frequency ranges with the best SNR we can apply more signal power, while in the frequency ranges with lower SNR less signal power is spent (the 'water-pouring' principle) [Bingham]. Examples of OFDM applications include wireless LANs for data connections over radio channels, and (A)DSL for data connections over the plain old telephone system (POTS).

For the above reasons, some publications suggest the use of OFDM for communication over (for example) backplane PCBs with deep spectral nulls in their transfer function [Amirkhany-1]. However, due to the very high bandwidth (in the GHz range) of such links such a system can not be implemented in a similar way to that in the above two examples, in which the common implementation termed 'discrete multitone' (DMT) is used. In a DMT implementation, A-to-D converters and D-to-A converters convert from the analog to the digital domain and back, and most signal operations, like the fast Fourier transform (FFT), are carried out in the digital domain using digital signal processors.

As an alternative, in this chapter we look at the feasibility of an 'analog' OFDM system for data-transmission at gigabit rates (~10Gb/s) over backplanes. Such a system consists of analog mixers and analog integrate-and-dump blocks to first separate (demodulate) the OFDM subcarriers and then digitize them. This chapter is based on our existing publications [Schrader-2] and [Schrader-3].

This chapter aims to improve the understanding of the impact of timing non-idealities on such an 'analog' multi-tone system. First, in section 3.2, we briefly summarize the main principles underlying OFDM and its inherent advantage in terms of channel equalization. Section 3.3 then describes the proposed analog OFDM system. Next, section 3.4 characterizes the jitter that disturbs the system. We outline the different types of inter-carrier interference in section 3.5. Next, analytical calculations (section 3.6) and statistical simulations (section 3.7) are presented that give insight into the system-level trade-offs and possibilities of an analog OFDM system. More specifically, the effect of jitter and duty-cycle deviations on such a system is analyzed. We calculate SNRs and error rates for a number of different values for the RMS jitter, and for a number of different duty-cycle deviations. A bit rate limit is calculated and conclusions are drawn about the feasibility of such a system. In section 3.8 the results are compared with work from the literature. Finally conclusions are drawn in section 3.9.

3.2. OFDM principles

In OFDM, the transmitted data is modulated on several orthogonal subcarriers/tones. In order to avoid interference, these carriers have to comply with the orthogonality constraint, which is defined as (normalized) [Bingham]:

$$\frac{1}{T_{op}}\int_0^{Top} c_i(t)\cdot c_j(t)dt = \delta_{ij}, \quad \delta_{ij} = \begin{cases} 1, & i = j, \\ 0, & i \neq j, \end{cases} \tag{1}$$

where $c_{i,j}(t)$ are the carriers and T_{op} is the length of the receiver integration period ('orthogonality period'). Candidates for subcarrier/tone frequencies f_c are harmonic frequencies n/T_{op} with integer n. Integration over exactly T_{op} delivers perfectly orthogonal carriers.

The total bit rate b_{tot} of such a system will be:

$$b_{tot} = \frac{2}{T_s}\sum_{i=1}^{N_t} {}^2\log(N_{l,i}), \tag{2}$$

where $N_{l,i}$ is the number of DAC/ADC levels used on the i^{th} tone (where each tone is modulated with both an in-phase- and quadrature component - hence the factor two), N_t the number of tone frequencies in the symbol and T_s the total symbol length, including guard time T_{gt}. So $T_s = T_{op} + T_{gt}$.

OFDM has an inherent advantage in respect of equalization, as compared to linear equalization in e.g. a PAM system. In OFDM, the symbol rate is quite low compared to the channel bandwidth, due to the high number of subcarriers. Each subcarrier has a low bit rate. This, together with the guard time (cyclic prefix), simplifies the implementation of channel equalization [Bingham]. In OFDM, a Fourier transform is taken of the signal, the signal spectrum is obtained, and the channel transfer function is assumed to be flat within one single OFDM subcarrier. Channel equalization is then achieved through one complex multiplication of an equalization vector with the spectrum. The only constraint on the channel impulse response is that it fits within the cyclic prefix. To shorten the necessary cyclic prefix, an optional simple 'impulse response shortening' time-domain equalizer can also be added.

3.3. Practical proposal for 'analog OFDM' system architecture

In common Discrete Multi-Tone (DMT) implementations, the ADCs and DACs and the complex digital processing put limits on the bandwidth. In general, these systems are implemented using DSP techniques, but this is currently infeasible for a bandwidth in the gigahertz range. We introduce an architecture that solves some of these problems. A possible way to overcome the bandwidth limitation is to use analog multipliers and integrate-and-dump blocks. This combination effectively performs a Fourier transform in the analog domain.

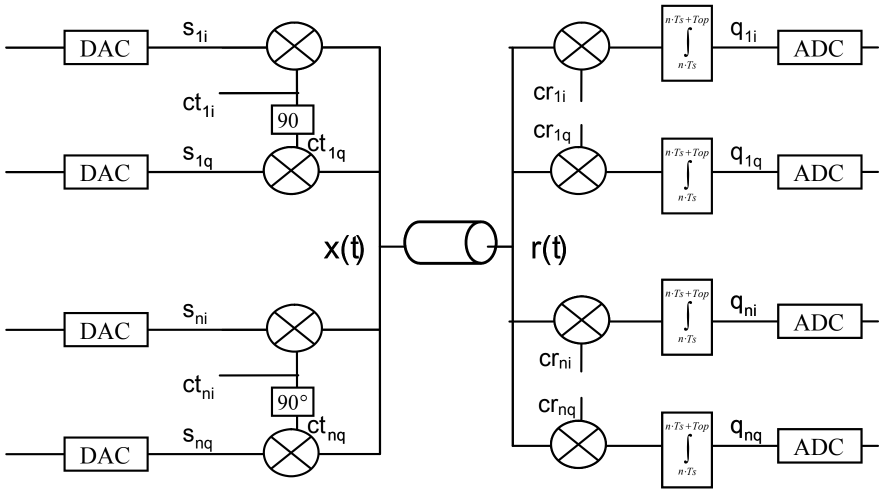

Fig. 1. Multi-carrier system using analog correlation

The multi-carrier communication system architecture that we study is shown in Fig. 1. On the left, the transmitter is shown and on the right, the receiver is shown. We use (passive or active) mixers for multiplication of the data streams with the carrier signals. For the integration over the symbol period, an integrate-and-dump block is used. ADCs and DACs can be added to provide more levels – and increase spectral efficiency. One architectural advantage now becomes apparent: parallelization is used for the converters and integrate-and-dump blocks, which relaxes bandwidth requirements.

In-phase and quadrature components of the subcarriers can be generated using a voltage-controlled oscillator. The multiple phases coming from the oscillator can also be used to control the integrate-and-dump blocks. Of course, a clock-and-data-recovery (CDR) block also needs be included in the receiver. This architecture puts a number of constraints onto the carrier waveforms that we can use. In an implementation with simple switching mixers, a sine wave on the local oscillator port will generate a square wave on the output. This will produce harmonics that fall onto other tone frequencies, creating unusable areas in the spectrum. Because of the abovementioned problems, it is likely that such a system would perform best when only a low number of subcarriers is used. A solution to the problem could be the use of harmonic rejection mixers [Weldon].

The signals in Fig. 1 are defined as follows. The bit streams $s_{ni}(t)$ and $s_{nq}(t)$, chosen from $\{-A_{max}, A_{max}\}$, are modulated onto the (in-phase and quadrature) carrier signals $ct_{ni}(t)$ and $ct_{nq}(t)$ and summed up, resulting in the sum signal $x(t)$ which is put onto the transmission line. At the receiver side the received signal $r(t)$ is demodulated using a 'correlator receiver' consisting of a multiplication with locally generated (in-phase and quadrature) carrier signals $cr_{ni}(t)$ and $cr_{nq}(t)$ and an integrate-and-dump operation. The recovered (soft-)bit streams are $q_{ni}(t)$ and $q_{nq}(t)$. The transmitted signal $x(t)$ is now described as follows:

$$x(t) = \sum_{n=1}^{Nt} ct_{ni}(t) \cdot s_{ni}(t) + ct_{nq}(t) \cdot s_{nq}(t) \,. \tag{3}$$

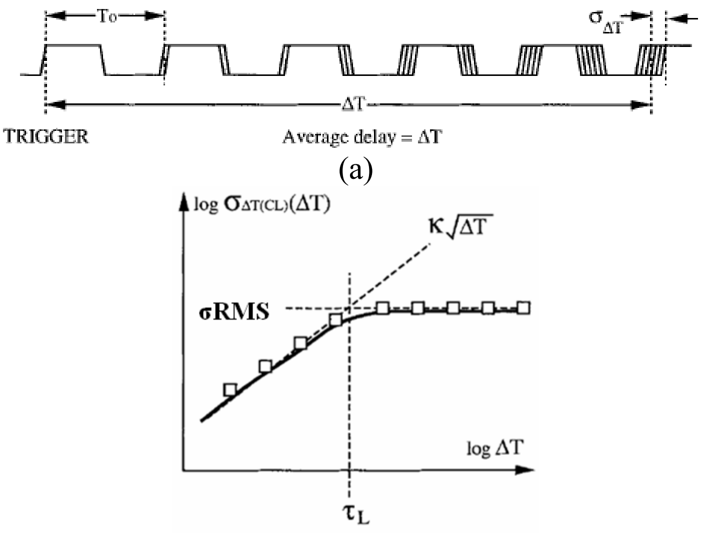

Fig. 2. Accumulated jitter in PLL [McNeill]. (a) Measurement technique. (b) Jitter versus measurement delay.

3.4. PLL jitter

We now determine the characteristics of the jitter that disturbs our analog OFDM system. It is assumed that the jitter coming from the PLL has a Gaussian amplitude distribution with an RMS standard deviation of σ_{RMS}. The value of this standard deviation is determined by the PLL noise and loop bandwidth. The PLL jitter is modeled as follows. In Fig. 2(a), the waveform at the PLL output is shown versus time. Starting on the left, we see that over time, the phase error accumulates. At delays shorter than the loop bandwidth time constant τ_L, the loop is too slow to correct the phase error. From [McNeill], the jitter variance as a function of measurement time in the left area of the plot is:

$$\sigma_t = \kappa\sqrt{\Delta T}\ , \tag{4}$$

where κ is an oscillator (time domain) figure of merit and ΔT is the accumulation time. Now because the PLL is locked, the phase error is bounded by the loop time constant τ_L. In Fig. 2(b), therefore, we can see that the variance of the accumulated phase error first increases versus time, and then becomes limited at σ_{RMS}, which is calculated as [McNeill]:

$$\sigma_{RMS} = \kappa\sqrt{\tau_L}\ . \tag{5}$$

In conclusion, at delays longer than the loop bandwidth time constant, the loop is able to track the reference and the variance is bounded to σ_{RMS}. A state-of-the-art jitter figure can be found in the literature: in [vdBeek], a 10GHz LC-based clock multiplier unit with an RMS jitter σ_{RMS} of 0.22ps at 81mW is described. For a ring oscillator, the jitter is somewhat higher: currently around 5ps RMS.

3.5. Types of inter-carrier interference

In this section, we outline the different types of inter-carrier interference that are analyzed. The multi-carrier receiver is a 'correlator receiver' (multiplication followed by integrate-and-dump) as opposed to the sampling receiver used in most PAM systems. The clock is extracted from the received signal using a clock & data recovery (CDR) circuit, usually PLL based. The locally generated carriers will not be exactly in-phase with the received signal due to PLL jitter. Also, frequency and duty-cycle deviations cause non-orthogonalities. The construction of orthogonal subcarriers in OFDM is quite sensitive to timing non-idealities. In a DMT system, all the timing is carefully observed: the ADC has a low jitter compared to the signal bandwidth and the digital FFT is theoretically perfect. The DMT system makes sure that all these timing non-idealities are absent or at least negligible compared to the channel bandwidth, but in the 'analog OFDM' system this is not always possible.

Because an OFDM system is in its nature quite sensitive to timing non-idealities, we analyze the impact of some of those non-idealities and see how they limit the achievable bit rate in the proposed system. Timing analyses were performed in e.g. [Zogakis], but these are based on a standard DMT system. We analyze our analog OFDM system here. We calculate the effect of jitter and duty-cycle deviations at the receiver side. The following types of inter-carrier interference (ICI) are considered:

(1) crosstalk between in-phase and quadrature signal at a given frequency,
(2) crosstalk between carriers at different frequencies.

This rest of this chapter deals with these different types of inter-carrier interference as follows. First, in section 3.6, we focus on jitter, which causes ICI of type (1). The impact of jitter is analyzed theoretically. Next, in section 3.7, statistical simulations are used to verify those theoretical results, and after that the impact of duty-cycle deviations, causing ICI of both type (1) and (2), is simulated statistically.

3.6. Impact of jitter on crosstalk between in-phase and quadrature signal at a given frequency

The goal of this section is to calculate the bit rate limit caused by crosstalk between I&Q components in a certain subcarrier, caused by jitter in the locally generated carrier. The analysis is based on 'correlation plots', which are introduced in the next sections. This presents an intuitive way of understanding the mechanism of effective amplitude variation of the integrator output caused by jitter. We assume the following:

- the locally generated carriers are:
    - perfect sinewaves
    - exactly frequency-locked
- the channel impulse response is a delta function.

When these assumptions are true, ICI of type (2) is effectively eliminated and we can focus entirely on (1). We also assume that a per-symbol jitter correction (for example based on a pilot-tone) is infeasible because of the high bandwidth.

This section is divided as follows. First, in section 3.6.1, we describe the concept of our jitter analysis. Next, in subsection 3.6.2, the necessary definitions are presented. Following that, we describe and draw the correlation plots (subsection 3.6.3), in order to visualize the I-Q crosstalk. After that, the probability of bit error is calculated (subsection 3.6.4), and finally the calculations of the limits on the achievable bit rate of our system are presented in section 3.6.5.

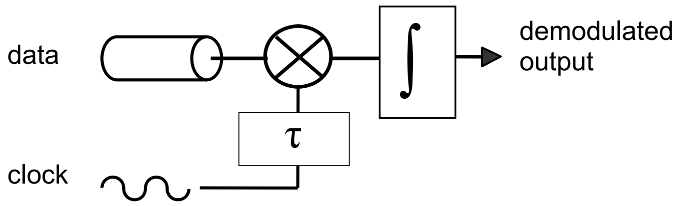

Fig. 3 – Modeling of jitter using delay τ.

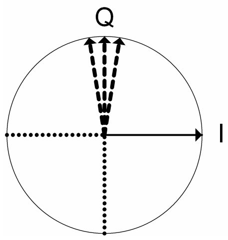

Fig. 4. Jitter in causing I-Q crosstalk. Solid line = I, dashed line = Q.

3.6.1. Concept of jitter analysis

Our analysis goal is to determine the change in the integrator output as a function of variations in τ, shown in fig. 3. Ideally, this τ should be zero, when the clock-and-data recovery (CDR) loop perfectly tracks the transmit clock and provides a carrier with a precisely correct phase. However in practice there is jitter in the receiver generated clock, as described above. We model the jitter in τ, which is thus 'jittering' around its ideal value of zero. This leads to crosstalk between in-phase and quadrature components of a certain subcarrier, and vice versa. This I-Q crosstalk is illustrated in Fig. 4: although we only want to demodulate the transmitted Q component, a small part of the I component will also be present in the demodulated signal.

3.6.2. Definitions

The receiver generated in-phase carrier $c_{r,i}(t)$ is defined as:

$$c_{r,i}(t) = A_r \sin(2\pi f_c t). \tag{6}$$

The transmitted, modulated subcarriers $s_i(t)$ and $s_q(t)$ (resp. in-phase and quadrature component) are defined as:

$$s_i(t) = A_i \sin(2\pi f_c t), \tag{7}$$

$$s_q(t) = A_q \cos(2\pi f_c t), \tag{8}$$

where A_i and A_q are chosen from interval [$-A_{max}$, A_{max}] and t is chosen from the interval ($-T_{gt}/2$, $T_{op}+T_{gt}/2$) (for one symbol). A guard time (cyclic prefix) T_{gt} is added to the symbol. The following analysis is valid for $-T_{gt}/2 > \tau > T_{gt}/2$.

3.6.3. Correlation plots

The receiver integrates over the time interval $(0, T_{op})$. As a first step, we calculate the (normalized) correlation $z_{ii}(\tau)$ between $s_i(t)$ and $c_{r,i}(t)$:

$$z_{ii}(\tau) = \frac{2}{T_{op}} \int_0^{T_{op}} s_i(t-\tau) \cdot c_{r,i}(t) dt = A_i A_r \cos(2\pi f_c \tau), \tag{9}$$

and the correlation $z_{qi}(\tau)$ between $s_q(t)$ and $c_{r,i}(t)$:

$$z_{qi}(\tau) = \frac{2}{T_{op}} \int_0^{T_{op}} s_q(t-\tau) \cdot c_{r,i}(t) dt = A_q A_r \sin(2\pi f_c \tau). \tag{10}$$

Mutatis mutandis these calculations (for the in-phase receiver component) deliver the same results for the quadrature receiver component $c_{r,q}(t)$. In fig. 5, example correlation functions are shown ($A_i=A_q=A_{max}$). The units on the x-axis are τ/T_c, where $T_c=1/f_c$. The maximum z_{ii} is (by definition) found at $\tau=0$ (optimum match between transmitter and receiver). At $\tau=T_c/4$ (90º phase shift) z_{qi} is maximum. It can be seen that the time shift between the local carrier and the received signal is very critical for optimum reception.

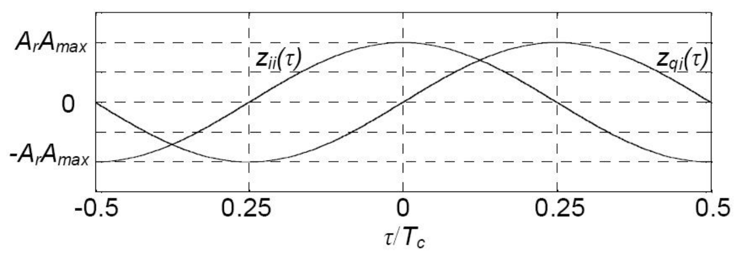

Fig. 5. Correlations $z_{ii}(\tau)$ and $z_{qi}(\tau)$ for $A_i=A_q=A_{max}$.

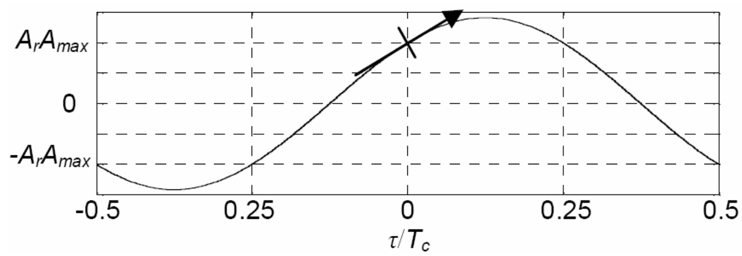

Fig. 6. Correlation $z_{s,Amax,Amax}(\tau)$ with summed signals, and derivative at optimum detection point (arrow) for $A_i=A_q=A_{max}$.

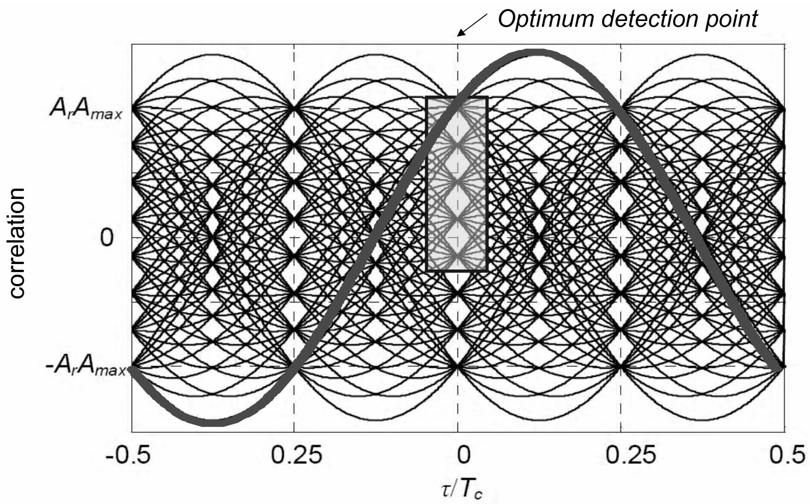

Fig. 7. Correlations $z_{s,Ai,Aq}(\tau)$ for all possible combinations of A_i and A_q.

Focusing on detection of the in-phase component, we calculate the correlation $z_{s,Ai,Aq}(\tau)$ of $c_{r,i}(t)$ with the summed transmitted signal, as a function of A_i and A_q,

$$z_{s,Ai,Aq}(\tau) = \frac{2}{T_{op}} \int_0^{T_{op}} \left(s_i(t-\tau) + s_q(t-\tau)\right) \cdot c_{r,i}(t)dt$$
$$= A_r\left(A_i \cos(2\pi f_c \tau) + A_q \sin(2\pi f_c \tau)\right). \tag{11}$$

This is shown in Fig. 6 (for A_i=A_q=A_{max}) together with the derivative at the optimum detection point. Next, we calculate $z_{s,Ai,Aq}(\tau)$ for all possible combinations where $-A_{max} < A_i < A_{max}$ and $-A_{max} < A_q < A_{max}$. Plotting all these correlations on top of each other looks a bit like a normal eye diagram. In Fig. 7 an example is shown where 3 bits are modulated on both the in-phase and quadrature component, resulting in 8 possible levels. The bold line is $z_{s,Amax,Amax}(\tau)$ (for A_i=A_q=A_{max}) as shown in Fig. 6.

Fig. 7 resembles an eye diagram but it is not the same. Like an eye diagram, these plots can actually be used, in a very similar way, to find the optimum detection moment and to analyze the effect of amplitude and time errors on bit error rate. However, note that the x-axis is not time but relative *time shift* between $r(t)$ and $c_{r,i}(t)$, in units of τ/T_c. The figure shows the effect of a time shift (away from the optimum detection point) on the integrator output.

The impact of a time shift depends on the steepness $y(\tau)$ of the lines around the optimum detection point. We need to calculate this steepness to be able to translate jitter into effective amplitude variation. The steepness is calculated as:

$$y(\tau) = \frac{d}{dt}\left(z_{s,Ai,Aq}(\tau)\right) = 2\pi f_c A_r \left(A_q \cos(2\pi f_c \tau) - A_i \sin(2\pi f_c \tau)\right). \tag{12}$$

For τ=0, $y(\tau)$ is completely determined by $A_r A_q$, so it can take on l discrete values, where l is the number of levels used in modulation. To be able to translate from time jitter into worst-case amplitude deviation, we calculate the maximum absolute steepness of these lines y_{max} as

$$y_{\max} = \max\left(\left| y(\tau) \;|_{\tau=0} \right|\right) = 2\pi f_c A_r A_{\max}. \tag{13}$$

It is shown in Appendix B that we can safely assume that the jitter accumulation *during* the integration period is negligible for $\kappa\sqrt{T_{op}} \ll T_c$, where T_{op} is the OFDM integration period (equal to the symbol duration minus the guard time), T_c the subcarrier period and κ, as said, is an oscillator figure of merit.

3.6.4. Probability of bit error

In this section, a 'tone error rate' P_e is calculated. Such a tone error occurs when either the in-phase component or the quadrature component of that specific tone (subcarrier) is detected incorrectly. The methodology to estimate the error probability is as follows:

- calculate the effective standard deviation of amplitude of integrator output (σ_{Aeq}) as a function of the jitter standard deviation (σ_{RMS}),
- calculate the SNR per tone from σ_{Aeq} and the distance between levels,
- calculate P_e using the cumulative normal distribution function.

The total system error rate will be limited by the worst performing tone. To avoid having one tone determine the system error rate, the system should be designed to have an equal error rate for each tone.

The receiver compares the integrator output to a number of (l-1) thresholds that are placed in between the amplitude levels. To calculate the error rate, we first need to calculate the probability that the received signal crosses the threshold between two amplitude levels. In Fig. 8, this is illustrated; t_n are the thresholds and s_n the signal points. Note that this figure is merely a zoomed-in version of Fig. 7.

The worst-case effective amplitude standard deviation σ_{Aeq} as a function of the jitter standard deviation is:

$$\sigma_{A_{eq}} = y_{\max}\sigma_t = 2\pi f_c A_r A_{\max}\sigma_t. \tag{14}$$

We can express the distance between levels 2d as a function of A_rA_{max} as:

$$2d = \frac{2A_r A_{\max}}{l-1}. \tag{15}$$

The error rate is a function of d/σ_{Aeq}, which is equal to the square root of the 'SNR per tone' SNR_{sm}. Expressing d/σ_{Aeq} in terms of f_c, σ_t and l gives:

$$\frac{d}{\sigma_{A_{eq}}} = \sqrt{SNR_{sm}} = \frac{1}{2\pi\sigma_t f_c(l-1)}. \tag{16}$$

To calculate P_e, we first calculate P_i, the error rate for the in-phase component, using the Gaussian distribution, and taking into account a factor (l-1)/l because the uppermost and lowermost levels have only one neighbor:

$$P_i = \frac{(l-1)}{l}\frac{1}{\sqrt{2\pi}}\int_{\frac{d}{\sigma_A}}^{\infty} e^{\left(-\frac{y^2}{2}\right)} dy = \frac{(l-1)}{l} Q\left(\frac{d}{\sigma_{A_{eq}}}\right), \tag{17}$$

where $Q(x)$ is the probability that a standard normal random variable with zero mean and unit variance exceeds x. Substituting (12) into (13) leads to:

$$P_i = \frac{(l-1)}{l} Q\left(\frac{1}{2\pi\sigma_t f_c(l-1)}\right). \tag{18}$$

The probability of error P_q for the quadrature component is equal to P_i, because the two components are orthogonal and at the same frequencies, and the noise is Gaussian. The (total) probability of a tone error P_e is:

$$P_e = 1-(1-P_i)^2. \tag{19}$$

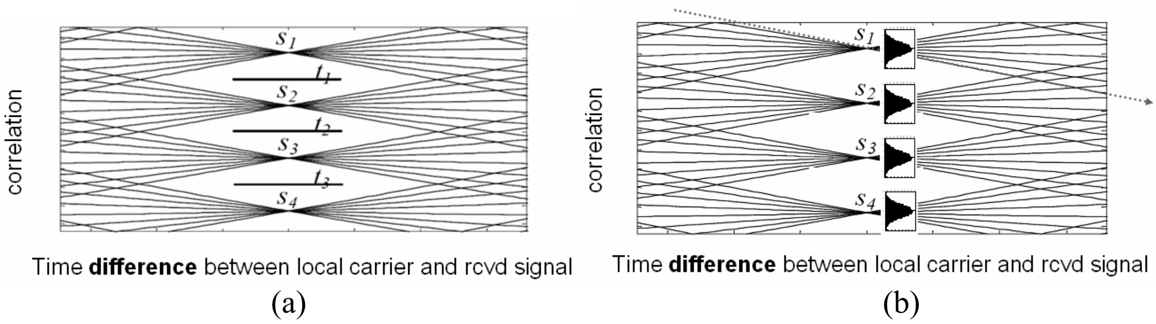

Fig. 8. Amplitude levels and thresholds. a) Levels and thresholds. b) Translation from timing noise to amplitude noise.

Now we can plot P_e (at a given σ_{RMS}) as a function of f_c for a number of different modulation depths n_b (=$\log_2(l)$, where n_b is expressed in bits). This is shown in Fig. 9 for σ_{RMS}=1ps. If necessary, we can convert from tone to bit errors, assuming the use of Gray code, so that one tone error will imply one bit error.

The error rate caused by jitter is a function of modulation depth n_b and subcarrier frequency f_c. The number of bits that can be modulated onto a carrier (for a given error rate) is limited by jitter, with higher frequency carriers being able to carry fewer bits. In an optimum multi-carrier system, the higher frequency carriers should have fewer constellation points to achieve the same error rate. This corresponds with results in [Zogakis].

3.6.5. Bit rate limits

To find the bit rate limit of the system, the "max. number of bits that can be modulated" $n_{b,max}$ was calculated as a function of σ_{RMS}, f_c and P_e, using a numeric solver on (18). Fig. 10 shows the outcome for three different values of σ_{RMS} = {0.1ps, 1ps, 10ps}, which corresponds to {*excellent, good, fair*}, for $P_e=1\cdot10^{-12}$.

It is important to know what the jitter limited maximum bit rate of such a multi-carrier system is. This is then compared to a PAM system with an equal bandwidth and error rate. In [Farjad-Rad] a PAM system is described that can achieve a bit rate of ~7Gb/s for an error probability of $\sim1\cdot10^{-12}$, with a bandwidth of 2GHz and an RMS jitter of 4ps. In our analysis, the upper bound on the multi-carrier system's bit rate is found by integration of $n_{b,max}$ over a 2GHz bandwidth and multiplying by two (because both in-phase and quadrature components are used). This delivers a bit rate limit of 14 Gb/s (for σ_{RMS}=4ps and $P_e=1\cdot10^{-12}$). Table 1 summarizes these findings.

The bit rate limit calculated for the multi-carrier system is two times higher than for the PAM system in [Farjad-Rad], but it will have to be corrected downwards for practical implementations. For one thing, the calculation does not include a cyclic prefix. The nonzero duration of the (shortened) impulse response of any practical channel necessitates the use of a guard time. In DMT systems, this guard time is quite a small percentage of the symbol duration because many subcarriers are used and symbols are long. In an analog OFDM system, due to the hardware parallelization with separate mixers, integrate-and-dump blocks and ADCs/DACs, it is more practical to use only few subcarriers. In that case the cyclic prefix could become long relative to the symbol duration. Furthermore, in an implementation with simple switching mixers, a sine wave on the local oscillator port will generate a square wave on the output. This will produce harmonics that fall onto other tone frequencies, creating unusable areas in the spectrum.

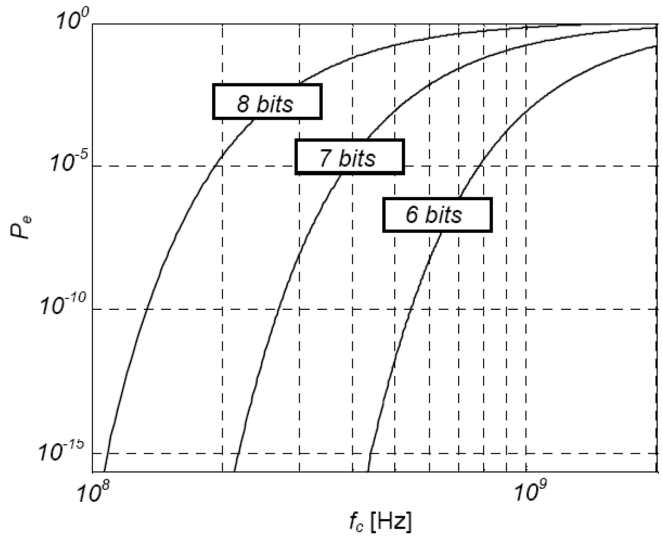

Fig. 9. Probability of error vs. carrier frequency for σ_{RMS}=1ps.

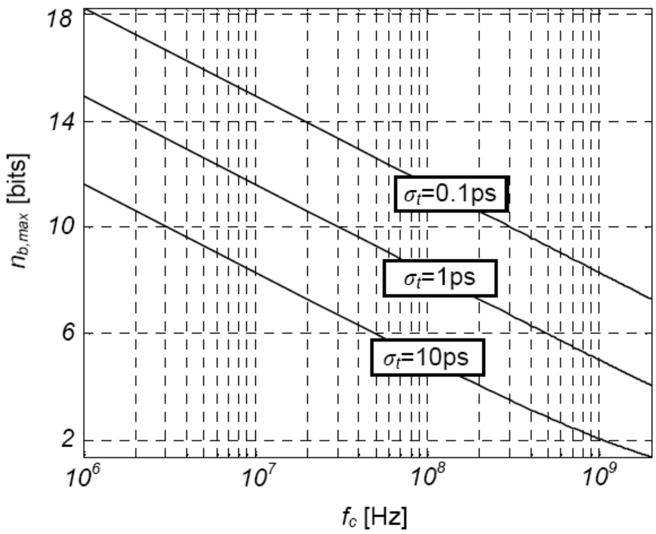

Fig. 10. Maximum number of bits that can be modulated vs. carrier freq. for P_e=$1\cdot10^{-12}$.

	PAM [Farjad-Rad]	**Analog OFDM**
BER	10^{-12}	10^{-12}
Bandwidth	2GHz	2GHz
RMS jitter	4ps	4ps
Capacity	7Gb/s (meas.)	14Gb/s (theory)

Table 1. Comparison between measured PAM system and proposed Analog OFDM system.

3.7. Statistical jitter simulations

In this section, we present statistical simulations regarding ICI of both type (1) and (2). First, subsection 3.7.1, we describe the use of statistical simulations to check the previous analytical calculations which estimated the influence of jitter on the error rate of the system (ICI of type (1)). Next, in subsection 3.7.2, the impact of duty-cycle deviations is analyzed, which causes both ICI type (1) and ICI type (2).

3.7.1. ICI type (1) as a consequence of jitter

We calculate an effective SNR as a function of jitter, and from this SNR calculate the error rate. It is again assumed that the jitter coming from the PLL has a Gaussian time distribution with an RMS variance of σ_{RMS}. Its size is determined by the PLL noise and loop bandwidth. From the calculations in the previous section, the effective SNR as a function of this jitter is expected to be dependent on carrier frequency f_c and number of levels N_l used in modulation. In the simulations, an OFDM symbol is used which is filled with only two subcarriers at one frequency f_c: the in-phase and the quadrature component. The length of the orthogonality period T_{op} is $1/f_c$. The received waveform is then multiplied with a randomly circularly shifted subcarrier. The circular shift is a white Gaussian random variable. The channel impulse response is a delta function, so the cyclic prefix length has no impact on the results. (Furthermore, the modeled receiver jitter only affects the carrier phase and does not modulate the symbol edges, which would have an impact for zero cyclic prefix length.)

We run the following simulations:

- f_c=0.5GHz, N_l=4, σ_{RMS}=10ps,
- f_c=2.5GHz, N_l=4, σ_{RMS}=10ps,
- f_c=0.5GHz, N_l=16, σ_{RMS}=10ps.

A jitter of 10ps is assumed because this enables us to detect errors over a short simulation (time step size=1ps). Statistical simulations are made with 500 symbols. We focus on the error rate for the in-phase component. We analyze crosstalk between in-phase and quadrature component of a single carrier as a function of variance in τ caused by jitter. The jitter was modeled by adding a white Gaussian random variable to the receiver time axis. The SNR per subcarrier values were calculated by sampling the data, demodulating the data and fitting it to a normal distribution. The fitting routine estimates the amplitude variance σ_A of the integrator output which is used to obtain the SNR per subcarrier SNR_{sm} as (see also previous section):

$$SNR_{sm} = \left(\frac{d}{\sigma_A}\right)^2 \tag{20}$$

where $2d$ is the distance between two adjacent levels. Next, the probability of error P_e for the in-phase component can be calculated as:

$$P_e = Q\left(\sqrt{SNR_{sm}}\right). \tag{21}$$

We use histograms of the integrator output to graphically show the variance σ_A. When we add a jitter of σ_{RMS}=10ps in the receiver generated carrier, and the frequency and number of levels are set at f_c=0.5GHz and N_l=4 levels (=2 bits) we can transmit data at a low BER. This is shown in Fig. 11. From the simulation, the calculated SNR_{sm}=25dB; this gives an excellent $P_e \ll 1\cdot 10^{-12}$. Using the formula derived in the previous section, we obtain SNR_{sm}=20.5dB. Analytical and statistical results correspond to within 5dB. This difference can be explained from the fact that the analysis takes the worst case steepness as per Eq. (13), and therefore arrives at a more pessimistic SNR estimation than the simulation. (The actual steepness is a function of the levels of the I and Q signals.)

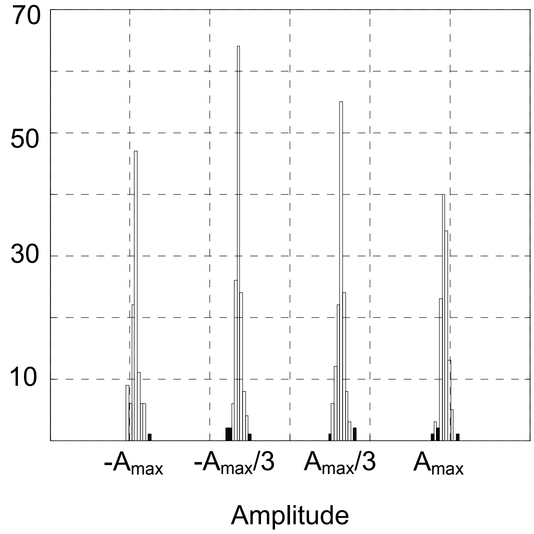

Fig. 11. Output hist. (jitter σ_{RMS}=10ps, f_c=0.5GHz, N_l=4).

However, when we try to increase the frequency to f_c=2.5GHz (number of levels remains N_l=4), the jitter starts to have a severe impact, causing SNR_{sm}=10dB, which gives a poor Pe=$1\cdot10^{-3}$. This is shown in Fig. 12. Calculated analytically, we obtain an SNR_{sm}=6.5dB.

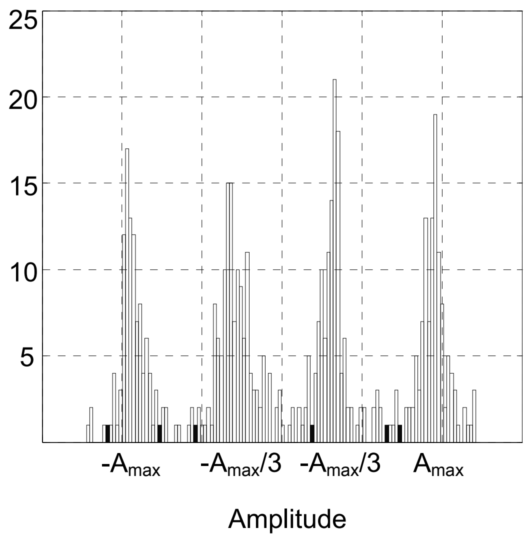

Fig. 12. Output hist. (jitter σ_{RMS}=10ps, f_c=2.5GHz, N_l=4).

A comparable jitter impact can be seen in Fig. 13 when we do not increase f_c (it remains at f_c=0.5GHz) but instead increase the modulation depth to N_l=16 levels. The signal-to-noise ratio per symbol SNR_{sm}=12dB, which gives an equally poor Pe=$1\cdot10^{-6}$. Using the formula derived in the previous section, we obtain an SNR_{sm}=6.5dB.

In conclusion, we observe that, for a given jitter RMS variance, low frequency tones can carry more bits than higher frequency tones for the same error rate. This confirms the previous analysis.

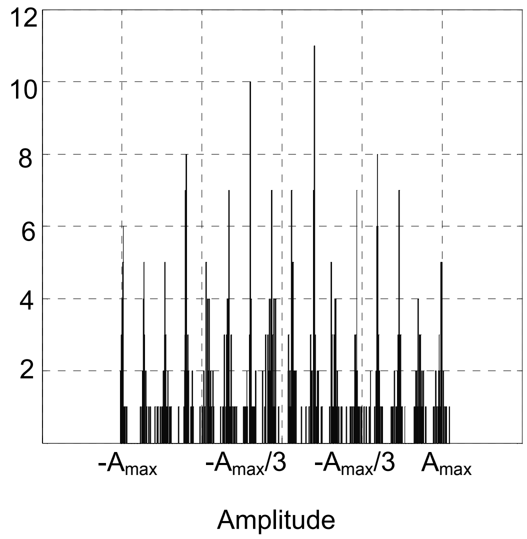

Fig. 13. Output hist. (jitter σ_{RMS}=10ps, f_c=0.5GHz, N_l=16).

A per-symbol jitter correction could be applied as in DMT systems, but the question is whether the electronics are fast enough to allow this. Leaving out the quadrature component would solve the jitter problems analyzed above, but at the cost of half the capacity. That would undo all of our gain in bit rate over the PAM system.

3.7.2. Impact of duty-cycle variations on carrier orthogonality

In this subsection we look at deterministic deviations and/or variations in the duty cycle. They can cause both type (1) and type (2) ICI. We simulate these effects for a system with two tone frequencies (f_2=2f_1) using square-wave carriers, where each frequency is modulated with both in-phase and quadrature components. (Therefore the total number of carriers is four.) The duty-cycle d of the receiver generated in-phase carrier $cr_{1,i}$ at f_1 is varied, while the duty-cycle of all the transmitted carriers is exactly 50%. Below, a short summary of the simulation setup is given.

Transmitter carriers:

- $ct_{1,i}$: f_c=f_1, in-phase component
- $ct_{1,q}$: f_c=f_1, quadrature component
- $ct_{2,i}$: f_c=f_2, in-phase component
- $ct_{2,q}$: f_c=f_2, quadrature component.

Receiver carrier:

- $cr_{1,i}$: f_c=f_1, in-phase component, deviations in duty-cycle.

We calculate the following correlations as a function of the duty-cycle of $cr_{1,i}$:

- $corr_1$ = between $cr_{1,i}$ and $ct_{1,i}$
- $corr_2$ = between $cr_{1,i}$ and $ct_{1,q}$
- $corr_3$ = between $cr_{1,i}$ and $ct_{2,I}$
- $corr_4$ = between $cr_{1,i}$ and $ct_{2,q}$.

These are all the possible correlations for this two-tone system.

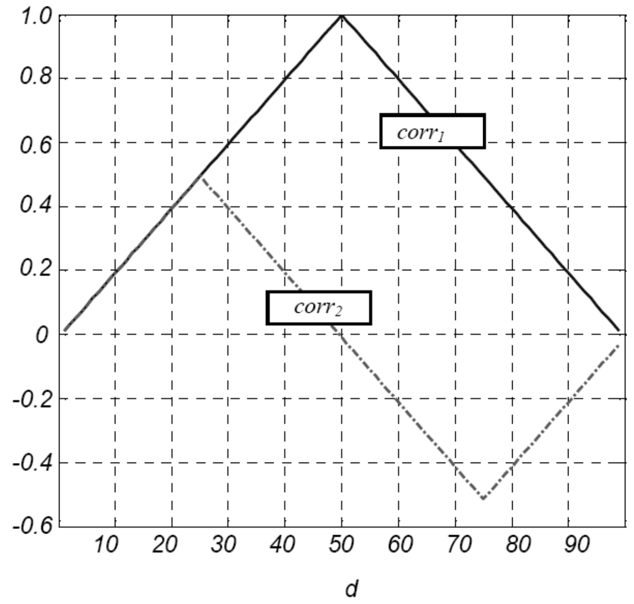

Fig. 14. $corr_1$ and $corr_2$ versus duty cycle d.

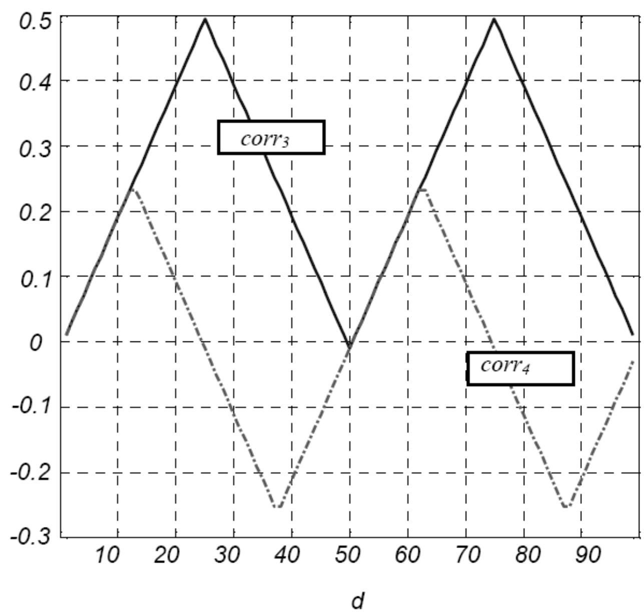

Fig. 15. $corr_3$ and $corr_4$ versus duty cycle d.

Fig. 14 shows the correlation of $cr_{1,i}$ with the desired transmitted signal $ct_{1,i}$ and with the quadrature component $ct_{1,q}$ at that same frequency (respectively $corr_1$ and $corr_2$). Fig. 15 shows the correlation of $cr_{1,i}$ with the double frequency carriers $ct_{2,i}$ and $ct_{2,q}$ ($corr_3$ and $corr_4$ respectively). The values were normalized to one.

All deviations from the 50% duty-cycle introduce inter-carrier interference (crosstalk) and lead to a limited SNR, as shown in Fig. 16. The peak at 50% corresponds to an infinite SNR.

The error rate as a function of the duty cycle is shown in Fig. 17. The observation to be made is that even this simple multi-carrier system is very sensitive to duty-cycle variations, with the error rate $P_e > 1\cdot10^{-6}$ for >5% variation. Also, in case of frequency mismatch or duty-cycle mismatch, inter-carrier interference with carriers at other frequencies will arise.

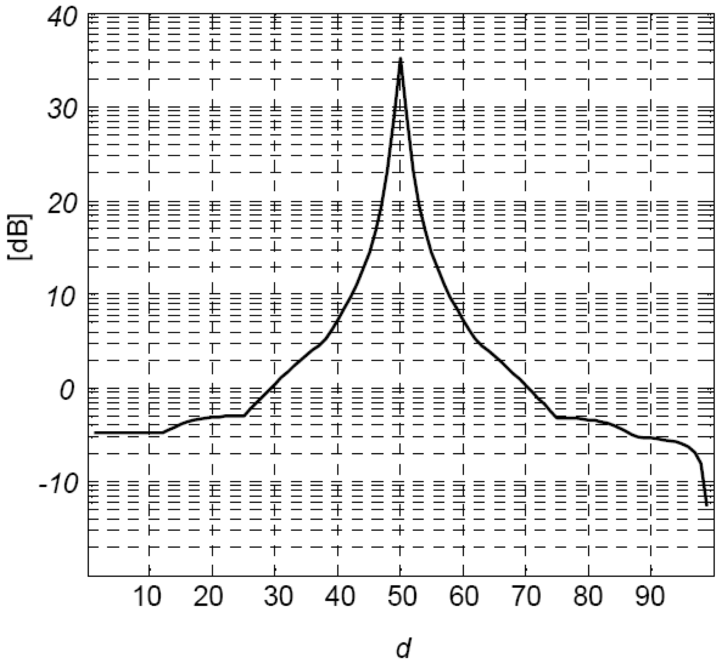

Fig. 16. SNR as a function of duty cycle *d.*

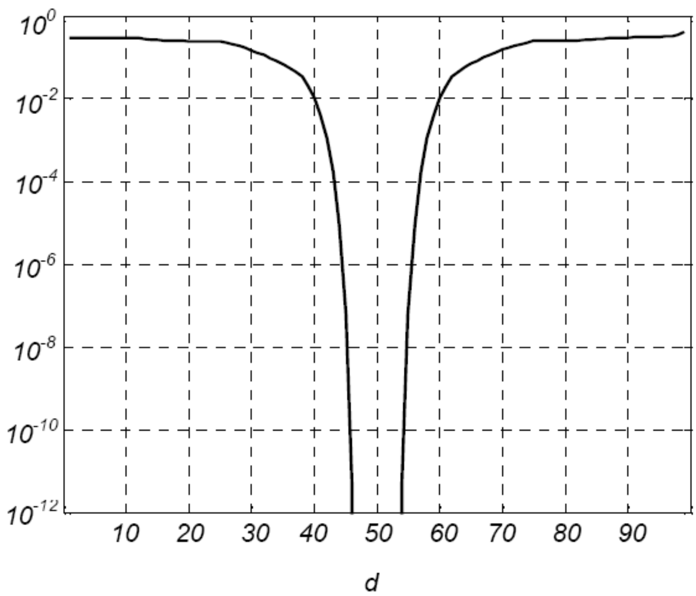

Fig. 17. Error rate P_e as a function of duty cycle *d.*

3.8. Related work from the literature

In [Amirkhany-1], work parallel to that presented above was carried out in the form of an analysis of an analog multitone (AMT) system. A system with 15 ADCs is proposed, which is analyzed using a convex optimization framework, with linear transfer matrices to model the inter-carrier interference (ICI). The outcome of the analysis is that an improvement of approximately a factor two in bit rate can be achieved over a PAM serial link, provided that "RF circuits with the characteristics specified … could be built in CMOS technology". As a follow-up on this work, in [Amirkhany-2], a transmitter was presented, but the receiver was not built. Instead, a very high-speed high-resolution ADC was used to sample the signal and all the data demodulation and equalization was done off-line. It remains to be seen whether such a receiver is feasible, especially in terms of jitter requirements. It is also concluded that multitone techniques are most advantageous on channels with spectral notches, and that ICI cancellation is one of the biggest challenges in building such analog multitone systems.

3.9. Conclusions

The feasibility of an 'analog OFDM' system is analyzed. A transceiver architecture for gigabit multi-carrier transmission over copper channels is discussed. Multiple parallel DACs and ADCs are used. Harmonics caused by switching mixers hinder the use of a large number of carriers. We have examined the impact of several timing non-idealities on system SNR, BER and capacity. Jitter, coming from the PLL, causes crosstalk between the in-phase and quadrature components. This limits the maximum bit rate which can be achieved, given a certain specification for the symbol error rate. The jitter is assumed to have a Gaussian amplitude distribution. It is concluded that low frequency tones can carry more bits than higher frequency tones for the same error rate. Using correlation plots, this can be understood. A jitter limit on the system bit rate is calculated by integrating the area under the plot of "maximum number of bits that can be modulated" versus carrier frequency. These analytical results were confirmed by running statistical simulations. Furthermore, duty-cycle deviations even cause crosstalk between carriers at different frequencies. A duty cycle deviation of more than 5% already causes the error rate of a simple two frequency multi-carrier system to drop below 10^{-6}.

It seems that traditional Pulse Amplitude Modulation (PAM) systems with a comparable bandwidth still are the better choice for channels with a loss that increases monotonously with frequency. OFDM techniques might still be attractive when the channel suffers from severe reflections, such as in some PCB tracks (and of course when it suffers from ingress noise as in ADSL systems).